Ana Rodrigues, Cátia Oliveira, Tiago Sousa, Delfim Pedrosa, Vítor Monteiro, João L. Afonso

"Unified Three-Port Topology Integrating a Renewable and an Energy Storage System with the Grid-Interface Operating as Active Power Filter,"

Unified Three-Port Topology Integrating a Renewable and an Energy Storage System with the Grid-Interface Operating as Active Power Filter

Ana Rodrigues
Centro ALGORITMI
University of Minho
Guimaraes, Portugal
arodrigues@dei.uminho.pt

Catia Oliveira
Centro ALGORITMI
University of Minho
Guimaraes, Portugal
c.oliveira@dei.uminho.pt

Tiago J. C. Sousa
Centro ALGORITMI
University of Minho
Guimaraes, Portugal
tsousa@dei.uminho.pt

Luis Machado
Centro ALGORITMI
University of Minho
Guimaraes, Portugal
lmachado@dei.uminho.pt

Joao L. Afonso
Centro ALGORITMI
University of Minho
Guimaraes, Portugal
jla@dei.uminho.pt

Vitor Monteiro
Centro ALGORITMI
University of Minho
Guimaraes, Portugal
vmonteiro@dei.uminho.pt

Abstract—**This paper presents the experimental validation of a unified three-port topology, integrating a renewable energy source (RES) and an energy storage system (ESS) (or an electric vehicle) with the grid-interface operating as active power filter (APF). The proposed topology is based on a three-phase grid-interface (whose role is to operate as a APF grid-tied inverter capable of compensating current harmonics, imbalanced currents and low power factor), on a RES-interface for solar photovoltaic (PV) panels (whose role is to extract the maximum power from the PV panels), and on an ESS-interface for batteries (whose role is to store/inject energy according to the power management of the electrical installation). The paper presents the control algorithms for each interface within the scope of the different operation modes allowed by the unified three-port topology. Simulation and experimental results are presented in order to validate the distinguishing aspects of the proposed unified three-port topology.**

Keywords—**Renewable Energy Source, Energy Storage System, Power Quality, Active Power Filter.**

I. INTRODUCTION

Most human activities depend on the use of electricity, therefore, as a basic need, it is important to develop new approaches not only to reduce costs, but also to produce and to manage electricity that meets the demand at all times. As the fossil fuels have harmful consequences in terms of environmental issues, the introduction of renewable energy sources (RES) has been contributing to transform the power grid [1][2][3]. However, in the perspective of compensating the intermittent power production from RES, the collaborative and effective integration of energy storage systems (ESS) is fundamental [4][5], as well as with electric vehicles [6]. The cooperation of RES with ESS is relevant, but the integration is performed through independent power converters (i.e., using independent grid-tied converters in terms of hardware resources) [7][8]. Moreover, this integration is performed at residential and industrial levels, where linear and non-linear loads are also presented with specific operating behaviors [4]. Therefore, additionally, the installation of an active power filter (APF) is fundamental to guarantee high levels of power quality from the power grid point of view. Consequently, based on this conventional approach, three distinct power grid interfaces (i.e., RES, ESS, and APF) are mandatory in the interface with the power grid [5]. However, analyzing in more detail, it is possible to identify that very similar grid-tied converters can be considered for the three cases. Therefore, the challenge is to use a single grid-tied converter, but with a shared dc interface since RES and ESS are naturally dc. Besides, the operation of the grid-tied converter as APF is independent of the dc-link operation, since it only needs to deal with the active power transactions between the power grid and the dc-link.

In this context, this paper proposes a unified three-port topology integrating a RES (solar PV panels) and an ESS (batteries) through a common dc-link with a single grid-interface (three-phase power grid). Regarding the grid-interface, it can operate as: (a) Active rectifier (absorbing power for the ESS); (b) Grid-tied inverter (injecting power from the RES or from the ESS); (c) APF combined or not with the operation as active rectifier or as grid-tied inverter. Similar concepts are already identified, mainly only based on the possibility to interface RES through an APF as demonstrated in [10][11][12]. A unified three-port topology is proposed in [13], but for single-phase installations. A multifunctional topology is validated only with simulations in [14] to interface RES and ESS with a single-grid interface, but it is a three-wire topology, which is limitative for operating in compliance with power quality standards. A computer simulation of a multifunctional system also to interface a RES and an ESS is presented in [15], but with the disadvantage that the ESS is connected to the dc-link without any dc-dc converter. Similarly, a computer simulation of a multifunctional system also to interface a RES and an ESS is presented in [16], but in this case the RES is connected to the dc-link without any dc-dc control converter. Taking into account the existing solutions, the main advantages of the proposed unified three-port topology are: (a) Three-phase four-wire topology, which can
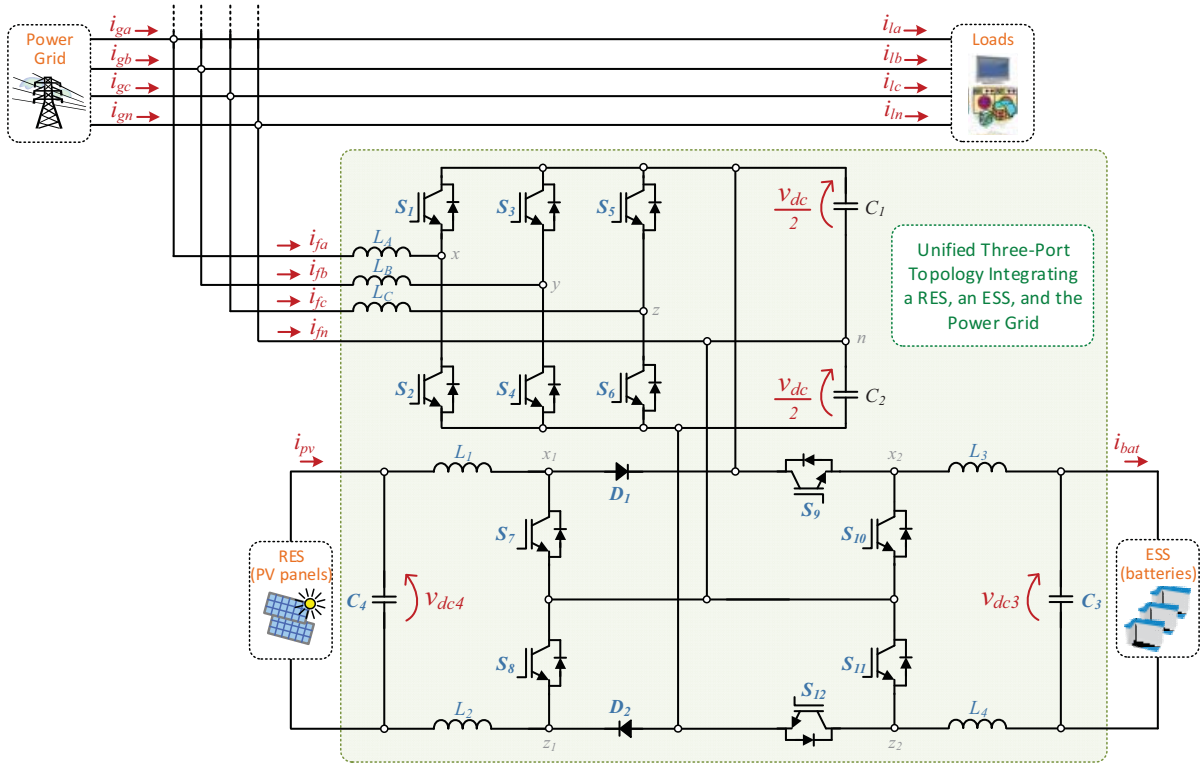
Fig. 1. Structure of the unified three-port topology integrating a renewable and an energy storage system with the grid-interface operating as active power filter.

compensate all the power quality problems related to currents; (b) Individual control of the RES interface and ESS interface using three-level dc-dc structures; (c) Experimental validation of the unified three-port topology. Moreover, the proposed topology integrates RES and ESS systems with the grid-interface operating to improve the power quality in terms of the grid currents. However, it can also be used to electrical mobility applications, namely electric vehicles. The structure of the proposed unified three-port topology is shown in Fig. 1.

II. UNIFIED THREE-PORT TOPOLOGY: CONTROL ALGORITHM

This section presents the control algorithm of each individual interface used in the unified three-port topology. The grid-interface consists of a three-phase four-wire bidirectional ac-dc converter, whereas the multilevel dc-dc converter is composed by two interfaces: a unidirectional used for the RES and a bidirectional used for the ESS. This unified three-port topology integrates these three interfaces with a common characteristic of having a single dc-link, without affecting the characteristics of each converter. The proposed system operates in different operation modes according to the battery modes (charging/discharging) and the energy delivered by the PV panels.

A. Bidirectional Grid-Interface

The bidirectional ac-dc converter is responsible for controlling the grid-interface and the dc-link, i.e., the grid-interface currents and the dc-link voltage. As shown, the topology is based on a four-wire three-leg voltage source structure, presenting the advantage of compensating the

neutral current without using an additional fourth leg [18]. According to the state of each switching device (IGBTs in the developed prototype), this converter can produce three voltage levels ($-v_{dc}$, 0, $+v_{dc}$). The current references for the grid-interface are calculated according to equation (1):

$$i_{fx}^* = \sqrt{2}\ \frac{p_{dc} + p_{pv} + p_{bat} + p_{load}}{3\,V_{gx}}\ p_{llx} - i_{lx},\tag{1}$$

where V_{gx} is the RMS grid voltage and i_{lx} the load current. As shown, the operating power is given by the sum of four individual powers: (1) Power necessary for the dc-link regulation (p_{dc}); (2) Power from the RES-interface (PV panels) (p_{pv}); (3) Power of the battery charging or discharging (p_{bat}); (4) Active power related with the operation of the loads (p_{load}). The power (p_{dc}) necessary to regulate the dc-link voltage (v_{dc}) to the reference voltage (v_{dc}^*) is obtained through two proportional-integral (PI) controllers, where each of them is used for each grid half-cycle (v_{dc1} is controlled to $v_{dc}^*/2$ when $v_g > 0$ and v_{dc2} is controlled to $v_{dc}^*/2$ when $v_g < 0$).

Depending on the operation mode of the bidirectional dc-dc converter (RES-interface and ESS-interface), the power demanded by the batteries (p_{bat}) is positive or negative (when the batteries are charging, p_{bat} is positive and when the batteries are delivering power to the grid, p_{bat} is negative). The active power (p_{load}) of the loads is obtained through the calculation of the load instantaneous power followed by a low-pass filter and it is used in order to mitigate the harmonic currents in the power grid. The four power components are used to calculate the reference currents through the Fryze-Buchholz-Depenbrock (FBD) power theory.

Comparatively to the *p-q* theory [17], the FBD theory is characterized by its simplicity due to the reduced number of calculations needed [19][20][21]. Moreover, in order to avoid the harmonic distortion of the grid voltage into the grid currents, for the calculation of the reference currents (i_{fx}^*), the fundamental component of each grid voltage (p_{llx}) is used. This is obtained using a phase-locked loop (PLL) algorithm presented in [22].

In order to control the currents on the grid-interface, a digital predictive current control was used. Equation (2) presents the digital predictive current control algorithm used for controlling the currents produced by the APF (i_f):

$$v_{cax} = v_{gx}[k] - \frac{L}{T_s}\left(i_{fx}^*[k] - i_{fx}[k]\right), \tag{2}$$

where v_{cax} is the reference voltage that the APF must synthesize for phase x ($x = \{a, b, c\}$), at the instant k, in order to control the current of the APF. On the other hand, $v_{gx}[k]$ is the instantaneous grid voltage, $i_{fx}^*[k]$ is the reference current of the APF and $i_{fx}[k]$ is the instantaneous current produced by the APF. Afterwards, the gate signals of the IGBTs are obtained using a sinusoidal pulse-width modulation (SPWM) technique, where a 20 kHz triangular carrier is used.

B. Bidirectional ESS-Interface

As mentioned above, the bidirectional ESS-interface is responsible for exchanging power between the dc-link and the ESS. It operates continuously and allows to charge and discharge the ESS with constant current or voltage (CC-CV method), depending on the operation mode. Besides, in accordance with the state of the IGBTs, this converter assumes three different voltage levels [23]. During the battery charging mode, the voltages synthesized by the dc-dc converter are determined as follows:

$$v_{conv\_dc3}[k] = V_{bat} - \frac{L_3 + L_4}{T_s}\left(i_{L3}[k] - i_{L3}[k-1]\right), \tag{3}$$

$$v_{conv\_dc4}[k] = V_{bat} - \frac{L_3 + L_4}{T_s}\left(i_{L4}[k] - i_{L4}[k-1]\right), \tag{4}$$

The control signals for the IGBTs S_9 and S_{12} are the result of the comparison between the synthetized voltages with two triangular carriers 180º phase shifted, similarly to an interleaved converter. On the other hand, when it is intended to discharge the batteries, and, thus, inject power into the grid, the voltages synthesized by the dc-dc converter are established as follows:

$$v_{conv\_dc3}[k] = V_{bat} - \frac{L_3 + L_4}{T_s}\left(i_{L3}[k+1] - i_{L3}[k]\right), \tag{5}$$

$$v_{conv\_dc4}[k] = V_{bat} - \frac{L_3 + L_4}{T_s}\left(i_{L4}[k+1] - i_{L4}[k]\right), \tag{6}$$

In this operation mode, the control signals for the IGBTs S_{10} and S_{11} are also obtained comparing the synthetized voltages with two triangular carriers 180º phase shifted.

C. Unidirectional RES-Interface

The unidirectional RES-interface is responsible for delivering the power from the RES to the dc-link. It operates continuously and it is controlled with the aim to extract the maximum power delivered by the PV panels, through a maximum power point tracking (MPPT) algorithm, incremental conductance in this case. Also in this case, the state of the IGBTs can be selected in order to the dc-dc converter operates with three different voltage levels [23]. The output voltages of the converter, v_{conv_dc1} and v_{conv_dc2}, are used in a fixed frequency predictive control. Applying the Euler method, it can be established the following digital implementation:

$$v_{conv\_dc1}[k] = V_{pv} - \frac{L_1 + L_2}{T_s}\left(i_{L1}[k+1] - i_{L1}[k]\right), \tag{7}$$

$$v_{conv\_dc2}[k] = V_{pv} - \frac{L_1 + L_2}{T_s}\left(i_{L2}[k+1] - i_{L2}[k]\right), \tag{8}$$

where $i_{L1}[k+1]$ and $i_{L2}[k+1]$ are the currents that are synthesized in instant $[k+1]$, representing thus, the reference currents. The control signals for the IGBTs S_7 and S_8 are obtained by comparing the synthesized voltages with two triangular carriers 180º phase shifted.

III. UNIFIED THREE-PORT TOPOLOGY: SIMULATION RESULTS

This section presents the main simulation results of the proposed unified three-port topology, which were obtained using the software PSIM 9.1. Fig. 2 shows the simulation results of the unified three-port topology operating in six modes: (a) Operation just as APF; (b) Operation as APF and with the ESS in the charging process; (c) Operation as APF and with the RES; (d) Operation as APF and with the ESS in the charging process and with the RES; (e) Operation as APF and with the ESS in the discharging process; (f) Operation as APF and with the ESS in the discharging process and with the RES.

Fig. 2 shows, for phase *a*, the power grid voltage and current (v_{ga}, i_{ga}) during the different stages. It is represented the phase *a* as exemplificative. The power exchanged between the loads, the power grid, the RES (PV panels) and the ESS (batteries) are also shown in Fig. 2, where p_g, p_{bat}, p_{pv}, p_{load} are, respectively, the power in the grid-interface, the power in the ESS-interface (batteries), the power in the RES-interface (PV panels), and the operating power of the load. During the first stage (from 0.26 s to 0.4 s) the system is operating as APF, where before the compensation the phase *a* grid current contains a high harmonic component with a total harmonic distortion (THD%) of 18.97%. After the compensation (at 0.3 s) the grid current is sinusoidal and in phase with the phase *a* grid voltage with a value of 16.9 A and a THD% reduced to 5.18%. Moreover, as it is possible to see, the consumed grid power (p_g) is equal to the power requested from the loads (p_{load}), 11.67 kW. In the second stage (from 0.4 s to 0.5 s) the system is controlled to compensate the power quality current problems in the power grid, which are introduced by the loads (harmonics and low power factor) and to discharge the batteries with a constant power, injecting approximately 1.5 kW into the power grid. Therefore, the grid power (p_g) is given by the difference between the load power (p_{load}) and the
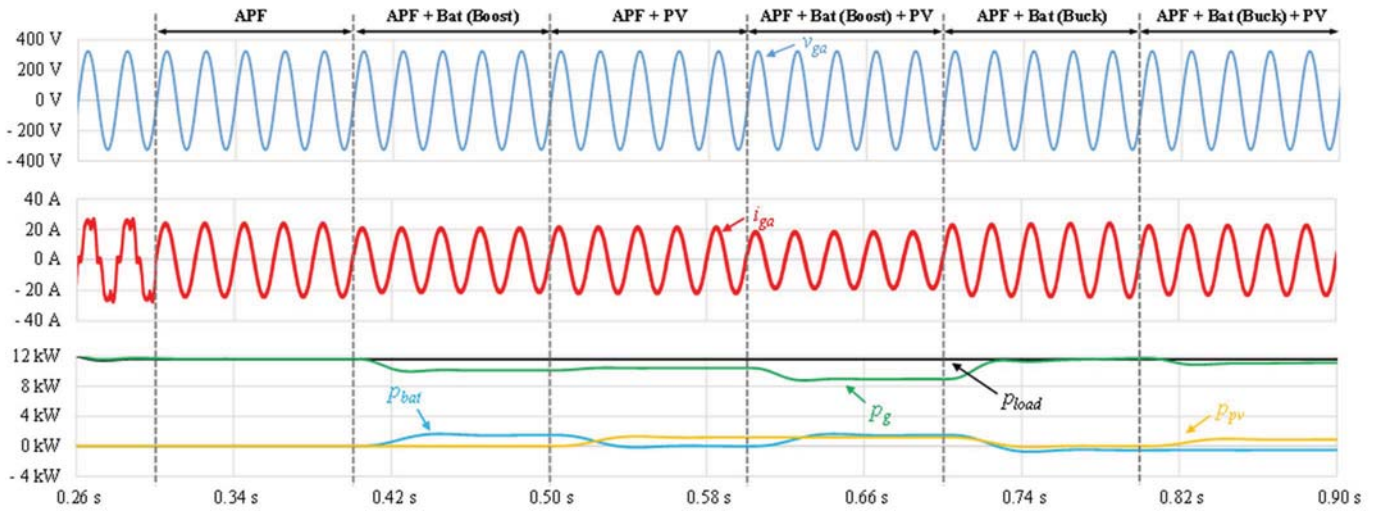
Fig. 2. Simulation results of the unified three-port topology: phase *a* grid voltage (v_{ga}) and current (i_{ga}), power consumed by the loads (p_{load}), power supplied by the power grid (p_g), power supplied by the PV panels (p_{pv}) and power in the batteries (p_{bat}).

batteries power (p_{bat}). During the third stage (from 0.5 s to 0.6 s) the system is responsible for extracting the maximum power from the PV panels and for injecting it in the power grid, while simultaneously compensating the power quality issues. The grid power (p_g) is the difference between the load power (p_{load}) and the PV power (p_{pv}). During the fourth stage of operation (from 0.6 s to 0.7 s) the APF controls the extraction of the maximum power from the PV panels and the discharging of the batteries for being injected into the power grid. Therefore, the grid currents are sinusoidal and balanced with a RMS value of 13 A and the grid power (p_g) is approximately 9 kW, which is given by the load power (p_{load}) subtracted by the PV power (p_{pv}) and the batteries power (p_{bat}). During the fifth stage of operation (from 0.7 s to 0.8 s) the power flows from the grid-interface to the ESS-interface and the current problems of the power grid are compensated. Thus, the batteries are charged with a constant power of approximately 570 W and the grid power (p_g) is the sum of the power consumed by the loads (p_{load}) with the batteries power (p_{bat}). The last stage (from 0.8 s to 0.9 s) controls the extraction of the maximum power from the PV panels, which is used to charge the batteries and the surplus is injected into the power grid. Therefore, the grid power (p_g) is the difference between the sum of the load power (p_{load}) with the batteries power (p_{bat}) and the PV power (p_{pv}). In all the operation modes, the APF is responsible for balancing the currents and compensate the current harmonics and the power factor of the electrical installation.

IV. UNIFIED THREE-PORT TOPOLOGY: EXPERIMENTAL VALIDATION

The developed prototype is presented in Fig. 3, where the main characteristics are presented in Table I. The ac-dc converter is composed mainly by three IGBT modules (SKM100GB12T4 from Semikron), three IGBT gate drivers (SKHI 22 A (R) from Semikron) and by passive filters (capacitors from the split dc-link and inductors to connect the converter in parallel with the power grid). The dc-dc converter

is composed by four IGBT modules (SKM50GB063D from Semikron), where two of them are used to interface with the ESS, whereas the remaining two modules are used to interface with the PV panels (although only two IGBTs are used, while in the other module are only used the antiparallel diodes). Moreover, the dc-dc converter is also formed by inductors to interface with the PV panels and with the batteries. On the other hand, the developed control system is composed by voltage sensors (CYHVS5-25A from Cheng Yang) and current sensors (LA-55P from LEM) and is based on the DSP TMS320F28335 from Texas Instruments. The main experimental results were obtained with a Yokogawa DL708E oscilloscope. It was used as load a three-phase diode rectifier with a RC filter, whose R value is 52 Ω and C value is 705 µF, in series with imbalanced resistive loads, whose values are 52 Ω, 78 Ω and 26 Ω, for phase *a*, *b* and *c*, respectively.

TABLE I. CHARACTERISTICS OF THE DEVELOPED PROTOTYPE

Parameter	Value
Power grid voltage (line-to-line)	400 V
Nominal power	10 kW
Nominal dc-link voltage	800 V
Nominal batteries voltage	300 V - 500 V
Nominal batteries current	15 A
Nominal PV voltage	300 V - 500 V
Nominal PV current	15 A
Switching frequency	20 kHz
Sampling frequency (f_s)	40 kHz
Coupling inductors (L_A, L_B, L_C)	2.4 mH
Dc-link capacitors (C_1, C_2)	8200 µF
Capacitor (C_3)	10 µF

Fig. 4 shows the currents consumed by the non-linear load, whose values are 5.7 A, 6.6 A and 8.4 A for phase *a*, *b* and *c*, respectively. As it can be seen, the grid currents (i_{ga}, i_{gb}, i_{gc}, i_{gn}) are imbalanced, presenting a RMS neutral current of 2.7 A. Moreover, the currents consumed by the load contain a high THD%, presenting a value of 20.9% (Fig. 5). As first

experimental test, the dc-link voltage regulation was performed to the reference average value of 400 V. Thereafter, the APF starts its operation, performing the compensation of the grid currents. After compensation, the dc-dc converter starts operating as boost in the RES-interface (extracting power from the PV panels) and as buck in the ESS-interface (charging the batteries) modes. The experimental results of this operation mode are presented in Fig. 6, where it can be seen the grid voltage (v_{ga}) and the grid current (i_{ga}) in phase a after compensation, whose THD% is reduced to 5% (Fig. 7). Besides, it is also possible to see the voltage and the current in the PV panels (v_{pv}, i_{pv}), whose current reaches 2 A, whereas the current in the batteries (i_{bat}) assumes the value of 3 A, as intended.
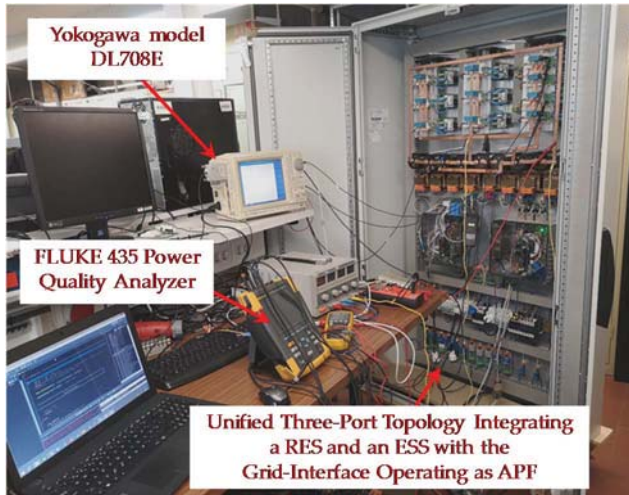
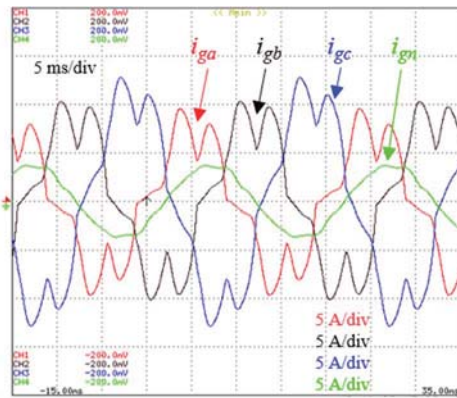Fig. 3. Developed prototype in a switchboard and experimental setup.

Fig. 4. Experimental results: Power grid currents (i_{ga}, i_{gb}, i_{gc}, i_{gn}) before compensation.

Afterwards, it was proceeded with the power injection into the power grid by the PV panels (with the RES-interface of the dc-dc converter operating as a boost-type) and batteries (with the ESS-interface of the dc-dc converter operating as a boost-type), following the same previously referred procedure. Fig. 8 shows, for phase a, the grid voltage and current (v_{ga}, i_{ga}) after compensation, with the current THD% being reduced to 8.2% (Fig. 9). In this operation mode it was defined a reference current of 2 A for the batteries and for the PV panels. As it can be seen, both the current in the batteries (i_{bat})

and the current in the PV panels (i_{pv}) are controlled to the value of the reference current.
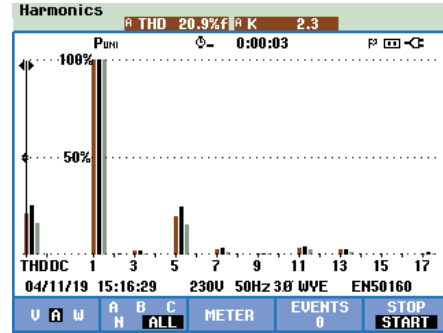

Fig. 5. Harmonic spectrum of the power grid currents before compensation.
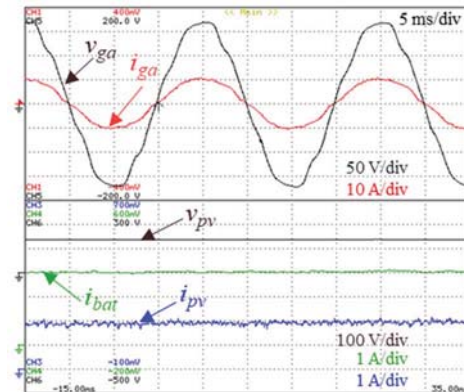

Fig. 6. Experimental results during batteries charging and energy extraction from the PV panels.
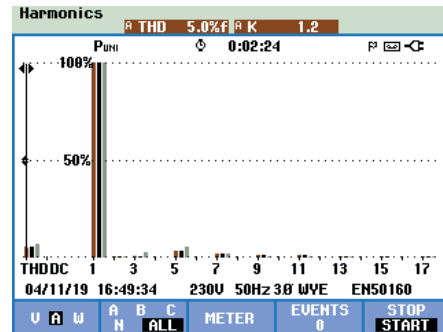

Fig. 7. Harmonic spectrum of the power grid currents after compensation and during batteries charging and energy extraction from the PV panels.
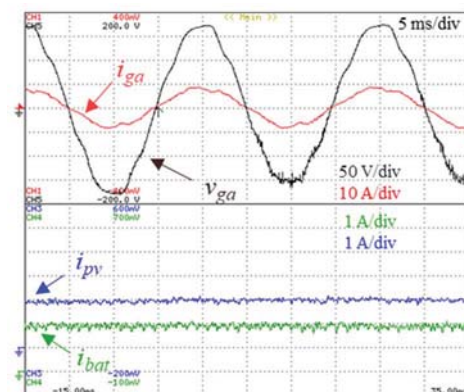

Fig. 8. Experimental results during batteries discharging and energy extraction from the PV panels.
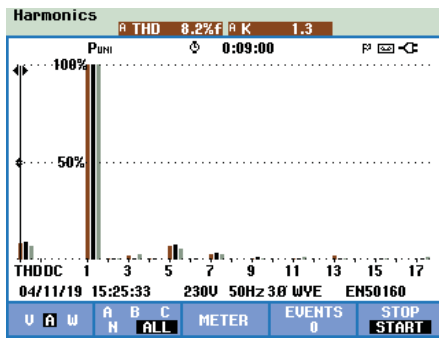
Fig. 9. Harmonic spectrum of the grid currents after compensation and during batteries discharging and energy extraction from the PV panels.

V. CONCLUSIONS

This paper presents a unified three-port topology interfacing solar photovoltaic (PV) panels and batteries (an energy storage system or an electric vehicle) with the power grid, where the grid-interface operates as active power filter (APF). It is composed by three stages sharing the same dc-link, and allows the power exchange between them while helping improve the power quality on the grid-interface. Throughout this paper, it is presented the topology, as well as the control algorithms. The system was experimentally validated in order to verify the correct functioning of the developed prototype operating in different modes. The experimental results validate the prototype and its control algorithms, showing that for all operation modes the grid currents are kept balanced and with a low total harmonic distortion (THD). Besides, the produced dc currents are constant, and with values according to the references, both in the batteries and in the PV panels.

ACKNOWLEDGMENT

REFERENCES

[1] T. Samad and E. Koch, "Automated Demand Response for Energy Efficiency and Emissions Reduction," IEEE PES Transmission and Distribution Conference and Exposition, pp.1-3, 2012.

[2] S. Pal, R. Verma, and R. Kumar, "Residential Demand Response Framework by Incorporating Renewable Energy Sources to Reduce Carbon Footprints," International Conference Inf. Technol. Electr. Eng., pp.443-448, 2018.

[3] Vítor Monteiro, Tiago J. C. Sousa, J. G. Pinto, João L. Afonso, "A Novel Front-End Multilevel Converter for Renewable Energy Systems in Smart Grids", ECOS 31st International Conference on Efficiency, Cost, Optimization, Simulation and Environmental Impact of Energy Systems, pp.1-12, Guimarães, Portugal, June 2018.

[4] N. Garimella and N. C. Nair, "Assessment of Battery Energy Storage Systems for Small-Scale Renewable Energy Integration," IEEE Region 10 Conference TENCON, pp.1-6, 2009.

[5] S. Vazquez, S. M. Lukic, E. Galvan, L. G. Franquelo, and J. M. Carrasco, "Energy Storage Systems for Transport and Grid Applications," IEEE Trans. Ind. Electron., vol.57, pp.3881-3895, 2010.

[6] Vítor Monteiro, José A. Afonso, João C. Ferreira, João L. Afonso, "Vehicle Electrification: New Challenges and Opportunities for Smart Grids," MDPI Energies, vol.12, no.1, pp.1-20, Jan. 2019.

[7] Vítor Monteiro, Tiago J. C. Sousa, M. J. Sepúlveda, Carlos Couto, Júlio S. Martins, João L. Afonso, "A Novel Multilevel Converter for On-Grid Interface of Renewable Energy Sources in Smart Grids", IEEE SEST International Conference on Smart Energy Systems and Technologies, Porto, Portugal, Sept. 2019.

[8] Vítor Monteiro, Jose Afonso, Tiago Sousa, Joao L. Afonso "The Role of Off-Board EV Battery Chargers in Smart Homes and Smart Grids: Operation with Renewables and Energy Storage Systems," Electric Vehicles in Energy Systems, Ali Ahmadian, Behnam Mohammadi-ivatloo, Ali Elkamel, SPRINGER, Chapter 3, pp.47-72, 2019.

[9] J. S. M. and J. L. A. Paulo Ferreira, Manuel Trindade, "Interfaces for Renewable Energy Sources with Electric Power Systems," Environ. 2010 Situat. Perspect. Eur. Union, pp.1-6, 2003.

[10] Ilango K., Manitha P.V., M. G. Nair, "An Enhanced Controller for Shunt Active Filter Interfacing Renewable Energy Source and Grid," IEEE ICSET Third International Conference on Sustainable Energy Technologies, pp.305-310, 2012.

[11] J. G. Pinto, R. Pregitzer, L. F. C. Monteiro, J. L. Afonso, "3-Phase 4-Wire Shunt Active Power Filter with Renewable Energy Interface," International Conference on Renewable Energies and Power Quality, no.5, pp.625-630, 2007.

[12] S. Sezen, A. Aktas, M. Ucar, E. Ozdemir, "A three-phase three-level NPC inverter based grid-connected photovoltaic system with active power filtering," International Power Electronics and Motion Control Conference and Exposition, pp.1331-1335, 2014.

[13] K. Akkala, R. Faranda, P. Milano, R. Italia, P. Sodini, H. Hafezi, "Distributed Storage System with Solar Photovoltaic Energy Source," in 2019 IEEE International Conference on Environment and Electrical Engineering and 2019 IEEE Industrial and Commercial Power Systems Europe (EEEIC / I&CPS Europe), pp.1-6, 2019.

[14] S. Rahmani, A. Hamadi, and H. Y. Kanaan, "A Multifunctional Power Flow Controller for Photovoltaic Generation Systems with Compliance to Power Quality Standards," IEEE IECON Anual Conference Ind. Electron. Soc., pp.894-903, 2012.

[15] S. Y. Mousazadeh, M. Savaghebi, A. Beirami, A. Jalilian, J. M. Guerrero, C. Li, "Control of a Multi-Functional Inverter for Grid Integration of PV and Battery Energy Storage System," IEEE SDEMPED International Symposium on Diagnostics for Electrical Machines, Power Electronics and Drives, pp.474-480, 2015.

[16] M. P. Behera, "Three-phase shunt connected photovoltaic generator for harmonic and reactive power compensation with battery energy storage device," IEEE IECON Annual Conference of the IEEE Industrial Electronics Society, pp.2408-2413, 2016.

[17] Edson Hirokazu Watanabe, João L. Afonso, José Gabriel Pinto, Luís Fernando Corrêa Monteiro, Maurício Aredes, Hirofumi Akagi, "Instantaneous p q Power Theory for Control of Compensators in Micro-Grids", Journal PRZEGLAD ELEKTROTECHNICZNY (Electrical Review), Issue: 06/2010, pp. 1-10, ISSN: 0033-2097.

[18] Filipe Ferreira, Luís Monteiro, João L. Afonso, Carlos Couto, "A Control Strategy for a Three-Phase Four-Wire Shunt Active Filter", IECON'08 - The 34th Annual Conference of the IEEE Industrial Electronics Society, Orlando, Florida, USA, 10-13 Nov. 2008.

[19] V. Staudt, "Fryze - Buchholz - Depenbrock : A time-domain power theory," IEEE International School on Nonsinusoidal Currents and Compensation, pp.1-12, 2008.

[20] João Afonso, Carlos Couto, Júlio Martins, "Active Filters with Control Based on the p-q Theory", IEEE Industrial Electronics Society Newsletter, vol.47, n.3, pp.5‑10, Sept. 2000.

[21] L. F. C. Monteiro, João L. Afonso, J. G. Pinto, E. H. Watanabe, M. Aredes, H. Akagi, "Compensation Algorithms based on the p-q and CPC Theories for Switching Compensators in Micro-Grids", Revista Eletrônica de Potência – SOBRAEP – Brazilian Power Electronics Society, ISSN 1414-8862, Vol. 14, no. 4, November 2009, pp. 259 268.

[22] L. G. B. Rolim, D. R. Da Costa, M. Aredes, "Analysis and software implementation of a robust synchronizing PLL circuit based on the pq theory," IEEE Trans. Ind. Electron., vol.53, no.6, pp.1919-1926, 2006.

[23] Vítor Monteiro, João C. Ferreira, Andrés A. Nogeira Melendez, José Afonso, Carlos Couto, João L. Afonso, "Experimental Validation of a Bidirectional Three-Level dc-dc Converter for On-Board or Off-Board EV Battery Chargers", IEEE IECON Industrial Electronics Conference, Lisbon, Portugal, Oct. 2019.